Application of the Finite-Difference Time-Domain Method to Sinusoidal Steady-State Electromagnetic-Penetration Problems

ALLEN TAFLOVE, MEMBER, IEEE

Abstract—**A numerical method for predicting the sinusoidal steady-state electromagnetic fields penetrating an arbitrary dielectric or conducting body is described here. The method employs the finite-difference time-domain (FD–TD) solution of Maxwell's curl equations implemented on a cubic-unit-cell space lattice. Small air-dielectric loss factors are introduced to improve the lattice truncation conditions and to accelerate convergence of cavity interior fields to the sinusoidal steady state. This method is evaluated with comparison to classical theory, method-of-moment frequency-domain numerical theory, and experimental results via application to a dielectric sphere and a cylindrical metal cavity with an aperture. Results are also given for a missile-like cavity with two different types of apertures illuminated by an axial-incidence plane wave.**

Key Words—**Finite-difference, time-domain, steady-state, plane wave, electromagnetic penetration, apertures, dielectric sphere, cylindrical metal cavity, missile-like cavity.**

I. INTRODUCTION

ELECTROMAGNETIC penetration problems are difficult to treat with many analytical or numerical methods because of the inability of these methods to simply deal with the effects of structure apertures, curvatures, corners, and internal contents. Usually, only relatively simple geometries and apertures are studied in an attempt to gain insight into the key penetration mechanisms and to allow an indirect estimate of the penetration for more complicated problems.

This paper reports the further development of a new approach for the direct modeling of the penetration of structures by continuous plane waves: the finite difference time-domain (FD–TD) solution of Maxwell's curl equations. The FD–TD method treats the illumination of a structure as an initial-value problem. At $t = 0$, a plane-wave source of frequency f is assumed to be turned on. The propagation of waves from this source is simulated by solving a finite-difference analog of the time-dependent Maxwell's equations on a lattice of cells, including the structure. Time-stepping is continued until the sinusoidal steady state is achieved at each cell. The field envelope, or maximum absolute value, during the final half-wave cycle of time-stepping is taken as the magnitude of the phasor of the steady-state field at each cell.

This method has two key advantages relative to available modeling approaches. First, it is simple to implement for complicated metal/dielectric structures because arbitrary electrical parameters can be assigned to each lattice cell using a data card deck. Second, its computer memory and running time requirement is not prohibitive for many complex structures of interest. In recent work, the FD–TD method has been shown capable of accurately solving for hundreds of thousands of unknown field components within a few minutes on an array-processing computer. Consistently, a ±1-dB accuracy relative to known analytical and experimental bench marks has been achieved for a variety of dielectric and metal geometries.

The objective of present work is to evaluate the suitability of the FD–TD method to determine the amount of electromagnetic coupling through an aperture into an enclosed conducting container and the interaction and coupling of the penetrating fields with internal electronics. Two specific container models are used for the evaluation. The first, a conducting cylinder with one open end. The other, the guidance section of a missile. Each of these two configurations is modeled to calculate the electromagnetic field coupled into the structure.

The ultimate aim of research in this area is two-fold. First, develop an easily used general code solving for the fields within arbitrary metal/dielectric structures having multiple apertures, while assuring a known bounded level of uncertainty. And second, develop a more sophisticated intuitive understanding of basic wave-penetration mechanisms in the time domain, such as transient propagation through beyond-cutoff cavity interiors, field buildup at edges, and convergence to the sinusoidal steady state.

This paper first briefly describes in Section II the basic theory behind the FD–TD method, referencing previous applications of this approach. This section will also establish the new elements of the latest work reported in this paper. In Section III, the FD–TD method is evaluated by comparison with classical analysis, a frequency-domain method-of-moments numerical approach, and experimental results. Finally, in Section IV, the FD–TD method is applied to the problem of a missile guidance-section shell having both nose and circumferential slot apertures and subjected to illumination by an axially directed incident plane wave.

II. THEORY

The FD–TD method is a direct solution of Maxwell's time-dependent curl equations. The goal is to model the

Manuscript received October 25, 1979; revised April 2, 1980. This work was supported in part under Contract F30602-77-C-0163 between Rome Air Development Center, Griffiss Air Force Base, New York, and I.I.T. Research Institute, Chicago, IL.

The author is with the I.I.T. Research Institute, Chicago, IL 60616. 312-567-4490.

0018-9375/80/0800-0191 $00.75 © 1980 IEEE

propagation of an electromagnetic wave into a volume of space containing a dielectric or conducting structure. By time-stepping, i.e., repeatedly implementing a finite-difference analog of the curl equations at each cell of the corresponding space lattice, the incident wave is tracked as it first propagates to the structure and then interacts with it via surface-current excitation, diffusion, penetration, and diffraction. Wave-tracking is completed when the desired late-time or sinusoidal steady-state behavior is observed at each lattice cell. The rationale for this procedure is that it achieves simplification by analyzing the interaction of the wavefront with portions of the structure surface at a given instant in time, rather than attempting a simultaneous solution of the entire problem.

Time-stepping for the FD–TD method is accomplished by an explicit finite-difference procedure due to Yee [1]. For a cubic-cell space lattice, this procedure involves positioning the components of E and H about a unit cell of the lattice, as shown in Fig. 1, and evaluating E and H at alternate half-time steps. In this manner, centered difference expressions can be used for both the space and time derivatives to attain second-order accuracy in the space and time increments without requiring simultaneous equations to compute the fields at the latest time step.

The finite-difference formulation of the FD–TD method allows the straightforward modeling of the surfaces and interiors of arbitrary dielectric or conducting structures. The structure of interest is mapped into the space lattice by first choosing the space increment and then employing a data card deck to assign values of permittivity and conductivity to each component of E. No special handling of electromagnetic boundary conditions at media interfaces is required because the curl equations generate these conditions in a natural way by themselves. Therefore, the basic computer program need not be modified to change from structure to structure. In this manner, inhomogeneities or fine details of the structure can be modeled with a maximum resolution of one unit cell; thin surfaces can be modeled as infinitely thin, stepped-edge sheets.

The explicit formulation of the FD–TD method is particularly suited for programming with minimum storage and execution time using recently developed array-processing computers. First, the required computer storage and running time increases linearly with N, the total number of unknown field components. Computer techniques (such as the method-of-moments) which require the solution of simultaneous equations usually have a storage requirement proportional to N^2 and a running time proportional to N^2–N^3 [2]. Second, since all FD–TD operations are explicit and can be performed in parallel, rapid array-processing techniques can be readily applied. As will be demonstrated later, these can be employed to solve for $10^5 - 10^6$ field components in a single FD–TD problem, as opposed to a maximum of about 10^3 field components for conventional approaches using simultaneous-equation solutions [2].

Yee applied the FD–TD method to compute the waveforms of TM and TE pulses scattered from infinitely long, rectangular cross section, conducting cylinders. Other workers

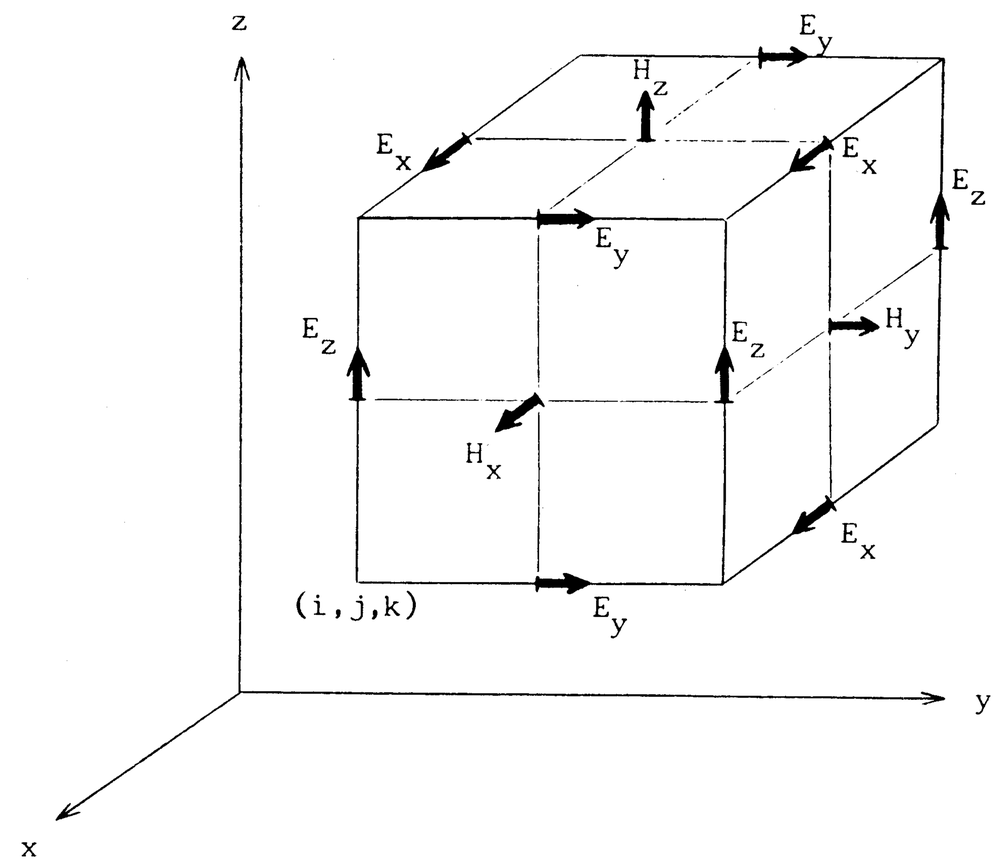

Fig. 1. Positions of the field components about a unit cell of the FD–TD lattice.

investigated electromagnetic-pulse interactions in time-varying inhomogeneous media [3], with metallic bodies of revolution [4], and with detailed models of aircraft [5]. Four distinct problems emerged in the process of adapting the FD–TD method to model realistic situations:

1) Lattice Truncation Conditions. The field components at the lattice truncation planes cannot be determined directly from the Maxwell's-equations analog and must be computed using an auxiliary radiative truncation condition. However, care must be exercised because this condition must not cause excessive spurious reflection of waves scattered outward by the structure modeled. The goal is to formulate truncation planes as close as possible to the structure (to minimize computer storage), and yet achieve virtual invisibility of these planes to all possible waves within the lattice.

2) Plane-Wave Source Condition. The simulation of either an incident plane-wave pulse or single-frequency plane wave should not take excessive storage nor cause spurious wave reflections. The former would occur if the incident wave is programmed as an initial condition; the latter would occur if the incident wave is programmed as a fixed field excitation along a single lattice plane.

3) Sinusoidal Steady-State Information. Such data can be obtained either by 1) directly programming a single-frequency incident plane wave or 2) performing a separate Fourier transformation step on the pulse waveform response. Both methods require time-stepping to a maximum time equal to several wave periods at the desired frequency. The second method has two additional requirements. First, a short-rise-time pulse suffers from accumulating waveform error due to overshoot and ringing as it propagates through the space lattice. This leads to a numerical noise component which should be filtered before Fourier transformation. Second, Fourier transformation of many lattice-cell field versus time waveforms (each probably extending over many hundreds of time steps) would significantly add to the total requirements for computer storage and execution time.

4) Total-Field versus Scattered-Field Formulation. A

choice exists in whether to finite-difference only the scattered field instead of the total field (at each lattice cell). The scattered-field approach may lead to a relatively superior lattice truncation condition [4]. However, the total-field approach may be more useful in determining the fields penetrating structures having shielding properties. In such structures, the total field at interior points can diminish to levels far below the incident. Scattered-field codes have traditionally run into numerical "noise" problems for such cases since they achieve interior-zone field reduction by the subtraction of nearly equal scattered and incident field quantities. Computed shielding of more than 30 dB may be difficult to achieve in this manner because of a residual "noise" floor inherent in this subtraction process. A total-field approach does not suffer from the subtraction-noise problem and hence is suitable for computing field penetration within shielded structures.

Previous work leading to this paper described efforts to solve the first three problems above for the case of a total-field FD–TD program employing a cubic-unit-cell space lattice [6], [7]. Simple truncation conditions were developed for two- and three-dimensional lattices that reduced the reflection coefficient of closely positioned truncation planes to the order of 0.1 for waves of arbitrary incidence. A plane-wave source condition was described that allowed generation of an arbitrary pulsed or sinusoidal incident wave without requiring any additional storage and without causing spurious wave reflections. Finally, it was shown that sinusoidal steady-state data could be computed using the FD–TD method by directly programming a single-frequency incident plane wave and time-stepping to the steady state over several periods of the incident wave. Observed accuracy for low-permittivity cylindrical dielectric geometries was ±1 dB at points of electric-field maxima, and ±1 lattice cell in locating electric-field maxima and minima, when the lattice-cell size was chosen to be less than 0.05 wavelength within the dielectric, as discussed in detail in [8].

In the latest work leading to this paper [8], additional FD–TD-method provisions were developed to allow accurate solutions for the sinusoidal steady-state fields penetrating metal structures having one or more apertures. This class of structures exhibits a different electromagnetic-penetration response than convex dielectric objects, due to such phenomena as aperture coupling, edge effects, and beyond-cutoff interiors. Further, the reflection coefficient of the metal surfaces modeled is larger than that of dielectric surfaces, leading to increased diffraction and the necessity for improved lattice truncation conditions. The new FD–TD-method provisions are now qualitatively discussed.

The first algorithm development involves the introduction of an anisotropic, lossy, air medium outside of the modeled structure to aid in reducing the effective reflection coefficient of the lattice truncation planes. Modeling of such a medium is possible because separate difference equations are available for each field vector component, thus allowing individual specification of loss to each field component. For the three-dimensional case, it is useful to specify an anisotropic electric-field loss σ_{ext} and/or an anisotropic magnetic field loss σ_{ext}* in the free-space region exterior to the structure. These loss terms are used only in the difference equations realizing $\nabla \times H = \sigma E + \epsilon \partial E/\partial t$ and $\nabla \times E = -\sigma^* H - \mu \partial H/\partial t$ for the electric- and magnetic-field components *not* present in the incident plane wave. The loss is selected to induce approximately $1/e$ decay of these field components as they propagate over a distance equal to the total dimension of the space lattice. In this manner, it is possible to avoid any exponential decay of the incident wave, which would lead to serious modeling error for structure sizes comparable to the $1/e$ distance. Further, the resulting modified scattered wave is reduced in amplitude upon reaching the lattice truncations and is progressively damped as its remnants reverberate between the structure and the truncations.

Application of this development has been found to be important in maintaining a ±1-dB accuracy of the FD–TD results for metal structures. To avoid the necessity of additional multiplications to realize the difference equations for the $\nabla \times E$ vector equation, it has been found useful to set σ^* equal to zero everywhere and rely upon only the use of σ_{ext} for suppression of scattered waves. However, it should be noted that a finite-value choice of σ_{ext}* in the region exterior to the structure of interest may provide more rapid damping of scattered waves. Furthermore, by selecting σ_{ext}* to equal $\mu_0\sigma_{ext}/\epsilon_0$, the effective steady-state wave impedance

$$Z = \sqrt{(j\omega\mu_0 + \sigma_{ext}^*)/(j\omega\epsilon_0 + \sigma_{ext})}$$

reduces to the lossless-case impedance

$$Z_0 = \sqrt{\mu_0/\epsilon_0}$$

allowing damping without significant dispersion or reflection as the sinusoidal steady state is approached.

The second algorithm development involves the introduction of a small isotropic conductivity σ_{int} within the interior of the modeled metal structure. The purpose of modeling the slightly lossy air is to cause the reverberating fields within the structure to converge more rapidly to the expected steady-state condition, especially for the case where the interior cavity volume is normally beyond cutoff at the frequency of the incident plane wave. In this case, the transient internal fields are highly reactive (carry little real-power flow) and quickly dissipate when forced to supply energy to maintain an electric-field distribution across a slightly lossy medium. As will be shown, accurate results are obtained in these circumstances when σ_{int} is chosen to provide an equivalent 10 dB of loss for a plane wave propagating the full length of the metal structure interior.

III. EVALUATION OF THE FD–TD METHOD

Dielectric and metal structures of convenient shape were chosen in order to compare the FD–TD method with classical techniques, a numerical body-of-revolution code, and experiment. The objective is to establish the level of accuracy of the FD–TD method by direct comparison to other results. This section will also illustrate the effects of σ_{int} in causing

improved convergence of cavity-interior fields to the sinusoidal steady state.

A. Dielectric Sphere

This problem involved the computation of the fields within a lossless dielectric sphere subjected to plane-wave irradiation. The sphere was assumed to have a diameter of 9 cm, a relative permittivity equal to 4.0, and be subjected to a $+y$-directed 2.5-GHz plane wave with field components $E_{z_{\text{inc}}}$ and $H_{x_{\text{inc}}}$.

The geometry of the sphere model relative to the $19 \times 39 \times 19$-cell, three-dimensional FD–TD problem lattice is depicted in Fig. 2 at the two lattice symmetry planes, $k = 19$ and $i = 19.5$. A lattice resolution $\delta = 0.3$ cm $= \lambda_d/20$ was used, with a time step $\delta t = \delta/2c = 5$ ps. The lattice coordinates internal to the sphere were determined by

$$[(i-19.5)^2+(j-20)^2+(k-19)^2]^{1/2} \leqq 15.$$

To reduce spurious wave reflections at the lattice truncations, a conductivity value $\sigma_{\text{ext}} = 0.1$ mho/m was assumed to act on E_x and E_y field components outside of the sphere.

Fig. 3(a) and (b) graph the computed, normalized values of two electric-field components near the sphere irradiation axis: $|E_y(19.5, j, 18)|/E_{z_{\text{inc}}}$ and $|E_z(19, j, 18.5)|/E_{z_{\text{inc}}}$. These values were obtained during the envelope observation period $460 \leq n \leq 500$, equivalent to the period 5.75–6.25 wave periods after the onset of irradiation. Fig. 3(a) and (b) also present the classical solution calculated using the frequency-domain, summed-mode series technique of Stratton [9]. As seen in the figures, the FD–TD solution located the positions of the peaks and nulls of the electric field with a maximum error of $\pm\delta$, or about ± 3 percent of the diameter of the sphere. The magnitude of each peak was determined with a maximum error of ± 1 dB.

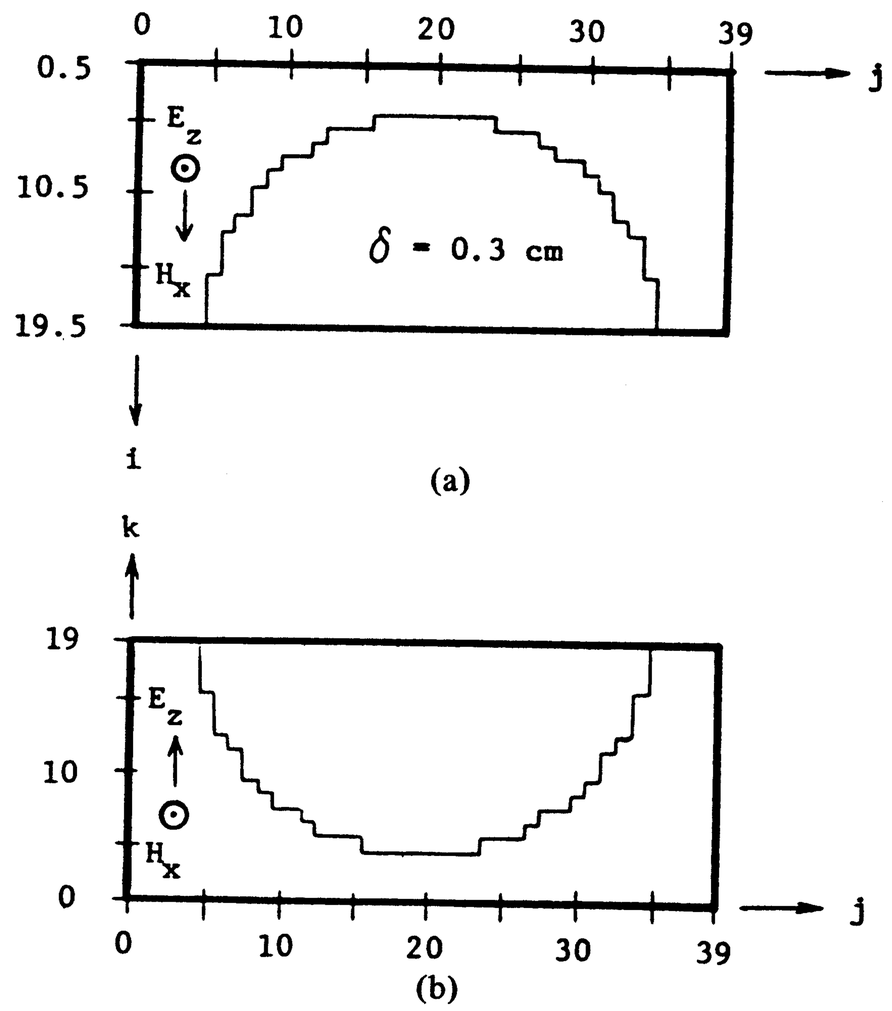

Fig. 2. FD–TD model geometry of a 9.0-cm diameter dielectric sphere. (a) Symmetry plane $k = 19$. (b) Symmetry plane $i = 19.5$.

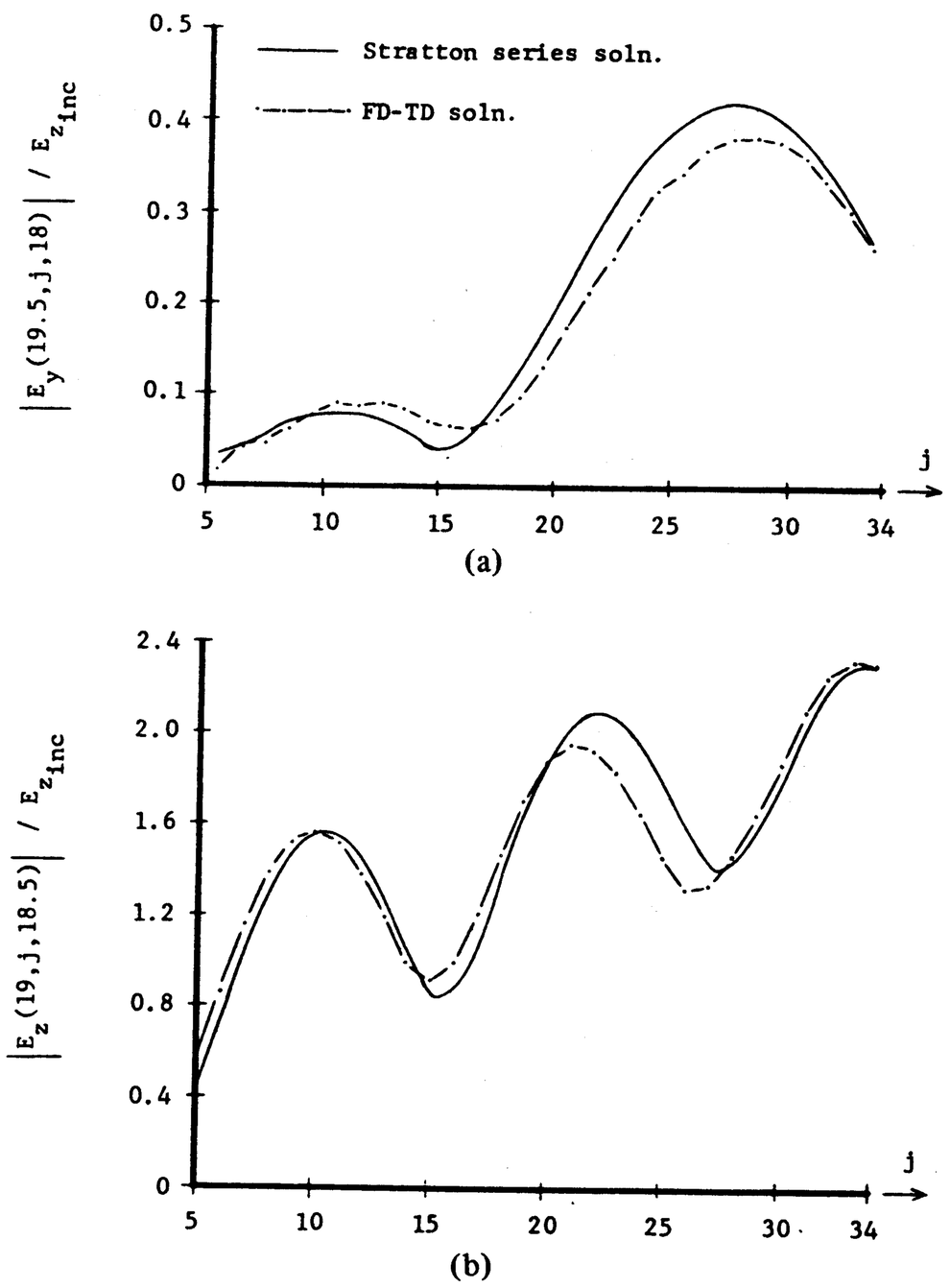

Fig. 3. Computed electric fields within the sphere of Fig. 2. (a) $E_y(19.5, j, 18)$. (b) $E_z(19, j, 18.5)$.

B. Cylindrical Metal Cavity

This problem involved the computation of the fields within a 19.0-cm diameter, 68.5-cm long, circular aluminum cylinder with one open end. The incident plane wave was assumed to have a frequency of 300 MHz, have the field components $E_{z_{\text{inc}}}$ and $H_{x_{\text{inc}}}$, and propagate along the cylinder $(+y)$ axis toward the open end. Since the cutoff frequency of the cylinder (as a waveguide) is above 900 MHz, the interior fields are expected to decay with distance from the aperture.

The geometry of the cylinder model relative to the $24 \times 163 \times 24$-cell (563,000 unknown field components) FD–TD problem lattice is depicted in Fig. 4 at lattice symmetry plane $k = 24$ and in Fig. 5 at a typical $j =$ constant plane cutting through the cylinder transversely. A lattice resolution $\delta = 0.5$ cm $= \lambda_0/200$ was used, with a time step $\delta t = \delta/2c = 8.33$ ps. The cylinder wall was specified by setting the conductivity σ equal to that of aluminum (3.7×10^7 mho/m) for individual E_x, E_y, and E_z components nearest the desired circular locus. This resulted in the modeling of the cylinder wall as an aluminum sheet having virtually zero thickness. A total of 72 punched data cards was needed to specify the cylinder model.

To reduce spurious wave reflections at the lattice truncations, a conductivity value $\sigma_{\text{ext}} = 0.01$ mho/m was assumed to act on E_x and E_y field components outside of the cylinder.

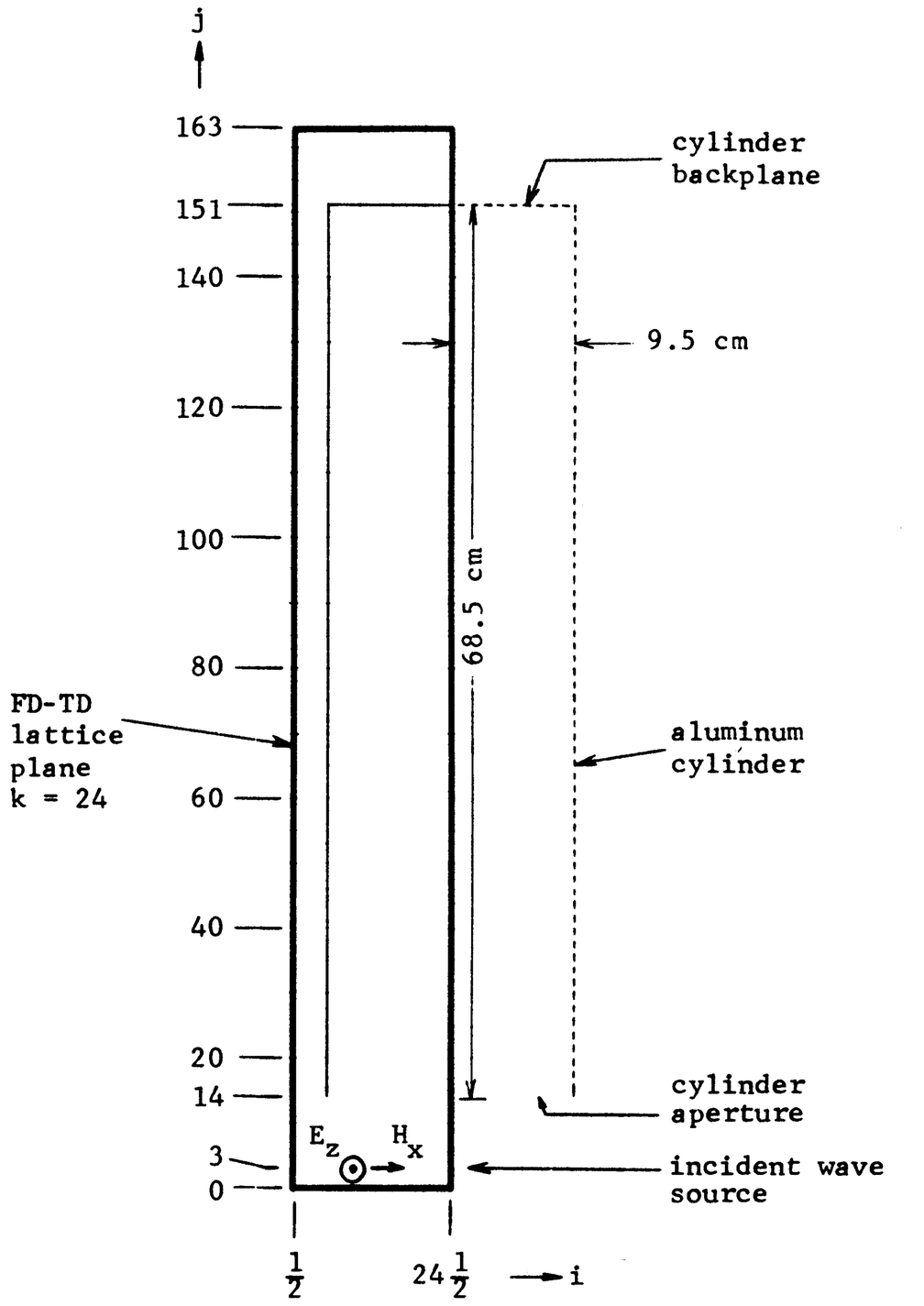

Fig. 4. FD–TD model geometry of a 19.0-cm diameter, 68.5 cm long, open-ended aluminum cylinder, as viewed at lattice plane $k = 24$ (horizontal symmetry plane).

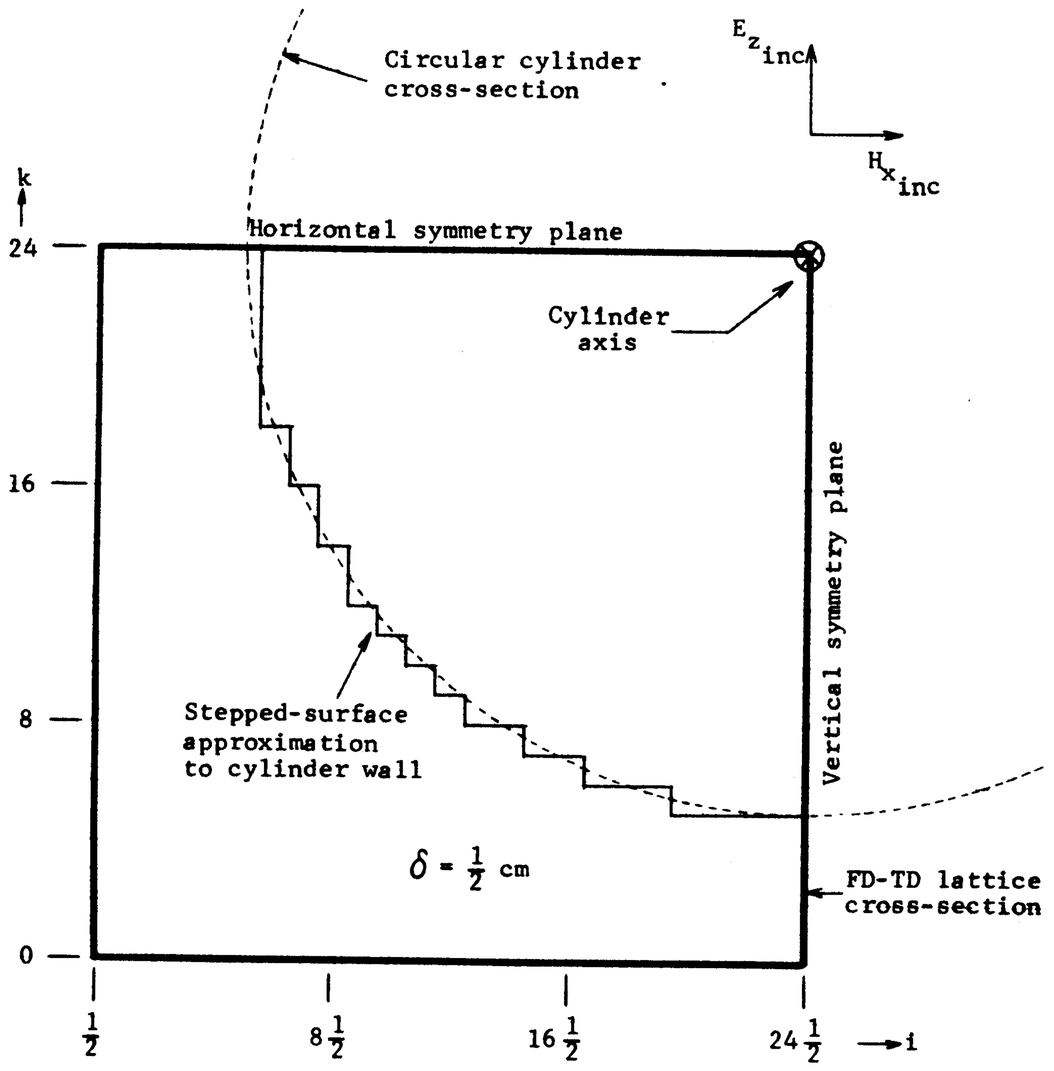

Fig. 5. Transverse cross section of the cylinder model of Fig. 4.

This value caused the exponential decay of E_x and E_y fields in the exterior region with an effective skin depth of about 110 lattice cells.

Two 800 time-step programs (each equivalent to 2.0 periods of the incident wave) have been run in order to investigate the rate of convergence of the computed fields to the sinusoidal steady state. The first program assumed lossless air within the cylinder; the second program assumed a small isotropic conductivity σ_{int} equal to 0.01 mho/m within the cylinder. The purpose of modeling the slightly lossy air was to cause the reactive fields within the cylinder to converge more rapidly to the expected beyond-cutoff condition. Each program required 10^6 words of memory and 3.5 min of central processor time on the Control Data STAR-100 computer, an array-processing machine.

Fig. 6(a) and (b) graph the computed total electric field, $|E_z/E_{z_{inc}}|$ (in decibels) along the axis of the cylinder for the case of $\sigma_{int} = 0$ and $\sigma_{int} = 0.01$ mho/m, respectively. In Fig. 6(a), curves are plotted for $n = 400$ and $n = 800$ time steps; in Fig. 6(b), curves are plotted for $n = 200$, $n = 400$, $n = 600$, and $n = 800$ time steps. Each curve gives the computed field envelope during the 200 time-steps period (0.5 cycle of the incident wave) before the specified value of n. In Fig. 6(b), it should be noted that, at 200 time steps, the incident wave penetrated only about 45 cm into the cylinder, causing the sharp downward break of the $n = 200$ curve. For all other curves, the incident wave penetrated fully to the cylinder backplane.

Comparing Fig. 6(a) and (b), it is seen that the use of σ_{int} caused the linear decibel slope at the cylinder aperture to lengthen from a maximum depth of 12.5 cm to more than 25 cm after 800 time steps. Further, the ultimate computed field attenuation increased from about 30 dB to almost 55 dB. This improvement in the convergence of the cylinder's internal fields to the expected cutoff condition is much more than the 11 dB of field decay that σ_{int} would cause for a plane wave propagating the full length of the cylinder.

Fig. 6(b) also indicates the rate of field convergence to the steady state under the condition of finite σ_{int}. Once the wave fields were established throughout the cylinder (curves $n = 400$, 600, and 800), the principal effect of an added 200 program time steps was the lengthening of the linear decibel slope extending from the aperture, and a consequent deepening of the field null within the cylinder. Noting the break points of the curves from the linear decibel slope, each 200 time-step increase is seen to have lengthened the slope by about 10 cm and decreased the residual internal fields by about 10 dB.

Using results of the FD–TD program, Fig. 7 graphs the computed $|E_z/E_{z_{inc}}|$ along the cylinder axis as a solid curve. The FD–TD results are after 800 time steps with $\sigma_{int} = 0.01$ mho/m (the $n = 800$ curve of Fig. 6(b)). For comparison, computed results using the frequency-domain, method-of-moments body-of-revolution code of Wilton and Glisson [10] are also shown, as well as experimental results [11].

From Fig. 7, it is seen that the FD–TD curve lies between the method-of-moments theory and the experimental results. The FD–TD and method-of-moments curves have nearly the same slope down to −55 dB, where the FD–TD curve levels

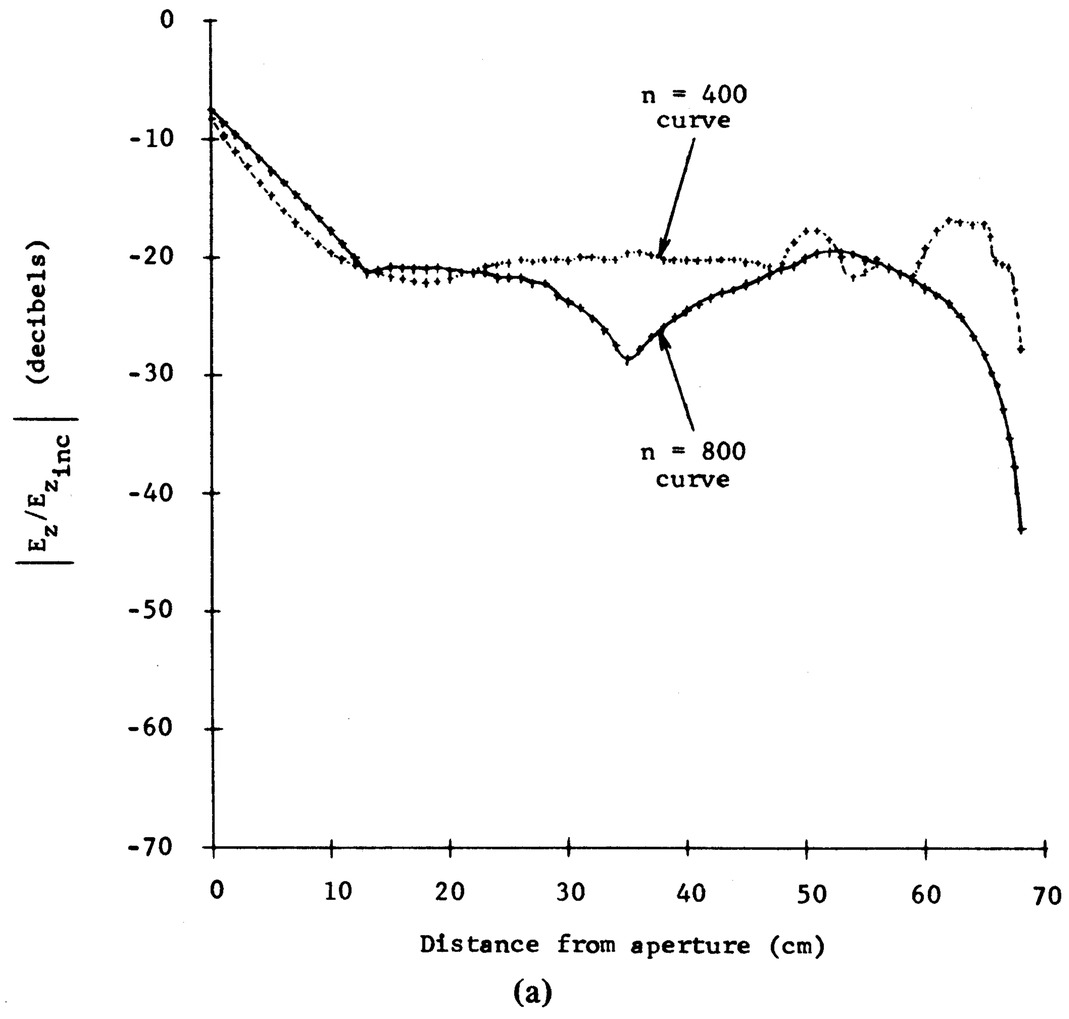

Fig. 6. Convergence of the FD–TD computed electric field along the cylinder axis. (a) $\sigma_{int} = 0$ case. (b) $\sigma_{int} = 0.01$-mho/m case.

off due to incomplete convergence after 800 time steps. Experimental results at points deeper than 15 cm within the cylinder are not shown because of measurement error due to inadequate suppression of radiated power at the third harmonic of the nominal test frequency, which excited a propagating mode in the cylinder [11], [12].

Figs. 8 and 9 graph contour maps of the computed field components at the cylinder's vertical and horizontal symmetry planes, respectively. All component magnitudes are normalized to either $|E_{z_{inc}}|$ or $|H_{x_{inc}}| = |E_{z_{inc}}|/377$, and are given as decibel numbers. Contours are plotted at exact 6-dB intervals by using a linear-interpolation method to determine the position of each contour between adjacent field-envelope points.

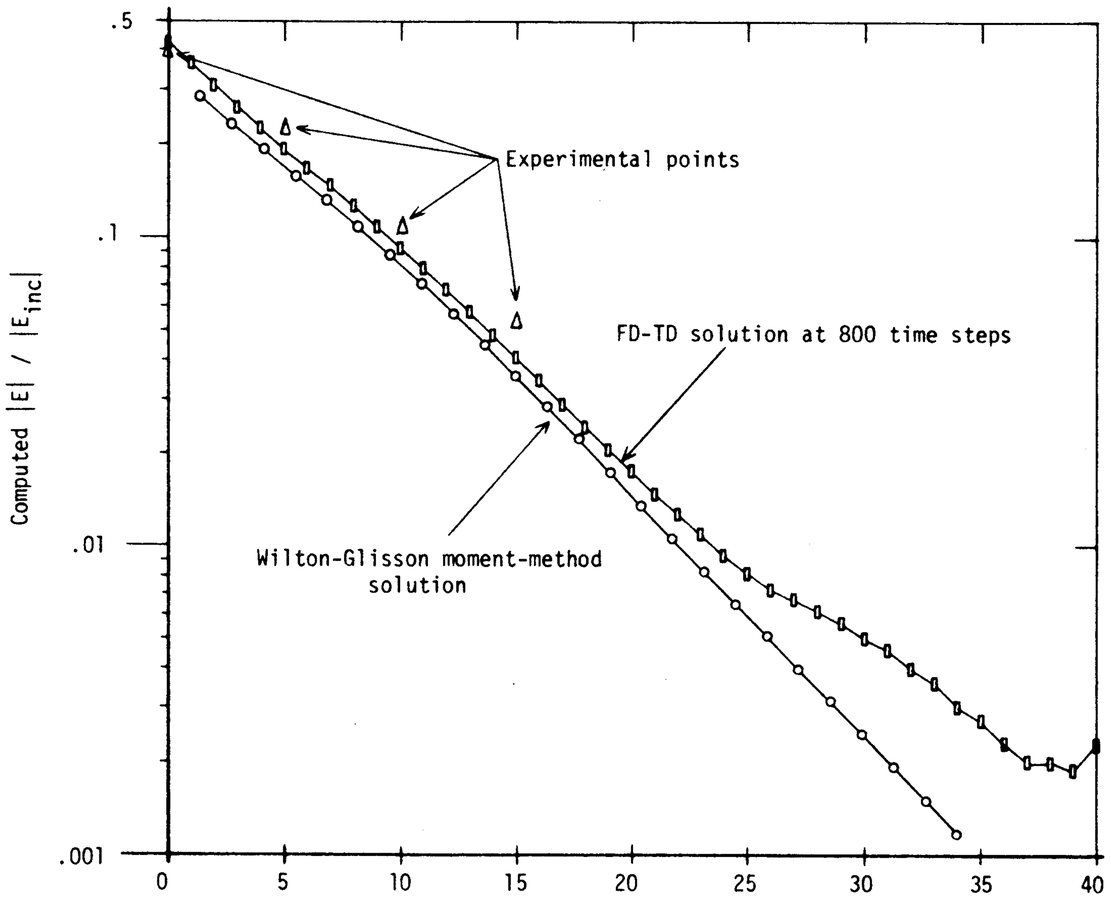

Fig. 7. Comparison of results for the electric field along the cylinder axis.

IV. NOSE CONE WITH THIN CIRCUMFERENTIAL APERTURE AND CIRCULAR NOSE APERTURE

This problem involved the computation of the fields within an aluminum nose cone (shown in Figs. 10 and 11) having two apertures, a circular one in the nose, and a circumferential sleeve fitting located 23-1/3-cm aft. The missile body geometry beyond the sleeve fitting was assumed to continue to infinity with a constant-cross section shape. The incident plane wave was assumed to have a frequency of 300 MHz with the field components $E_{z_{inc}}$ and $H_{x_{inc}}$, and propagate along the nose-cone $(+y)$ axis toward the nose aperture.

For this problem, the lattice of the aluminum-cylinder program was truncated to 24 × 100 × 24 cells (345 000 unknown field components) with an assumed resolution of δ = 1/3 cm = $\lambda_0/300$ and $\delta t = \delta/2c = 5.55$ ps. Again, a value of σ equal to 3.7×10^7 mho/m (aluminum) was assigned to the field components at the wall. A total of 464 data cards was required to specify the missile model.

For all lattice cells exterior to the model nose cone, the anisotropic conductivity σ_{ext} equal to 0.025 mho/m was assumed to help improve the lattice truncation conditions, as discussed earlier. This value of σ_{ext} caused the exponential decay of E_x and E_y fields in the exterior region with an effective skin depth of about 65 lattice cells. To speed convergence of the interior fields, as discussed in the previous section, the isotropic conductivity σ_{int} equal to 0.025 mho/m was selected for the cylinder interior. This allowed approximate convergence to the sinusoidal steady state after 900 time steps (1.5 cycles of the incident wave), giving a STAR-100 central processor time of 2.8 min (and memory requirements of 6×10^5 words) for the nose-cone run.

Figs. 12 and 13 graph contour maps of the computed field components at the nose cone vertical and horizontal symmetry planes, respectively. Contours are plotted at exact 10-dB intervals using linear interpolation. It is noted that the stepped-surface approximation of the smooth, tapered nose-cone wall

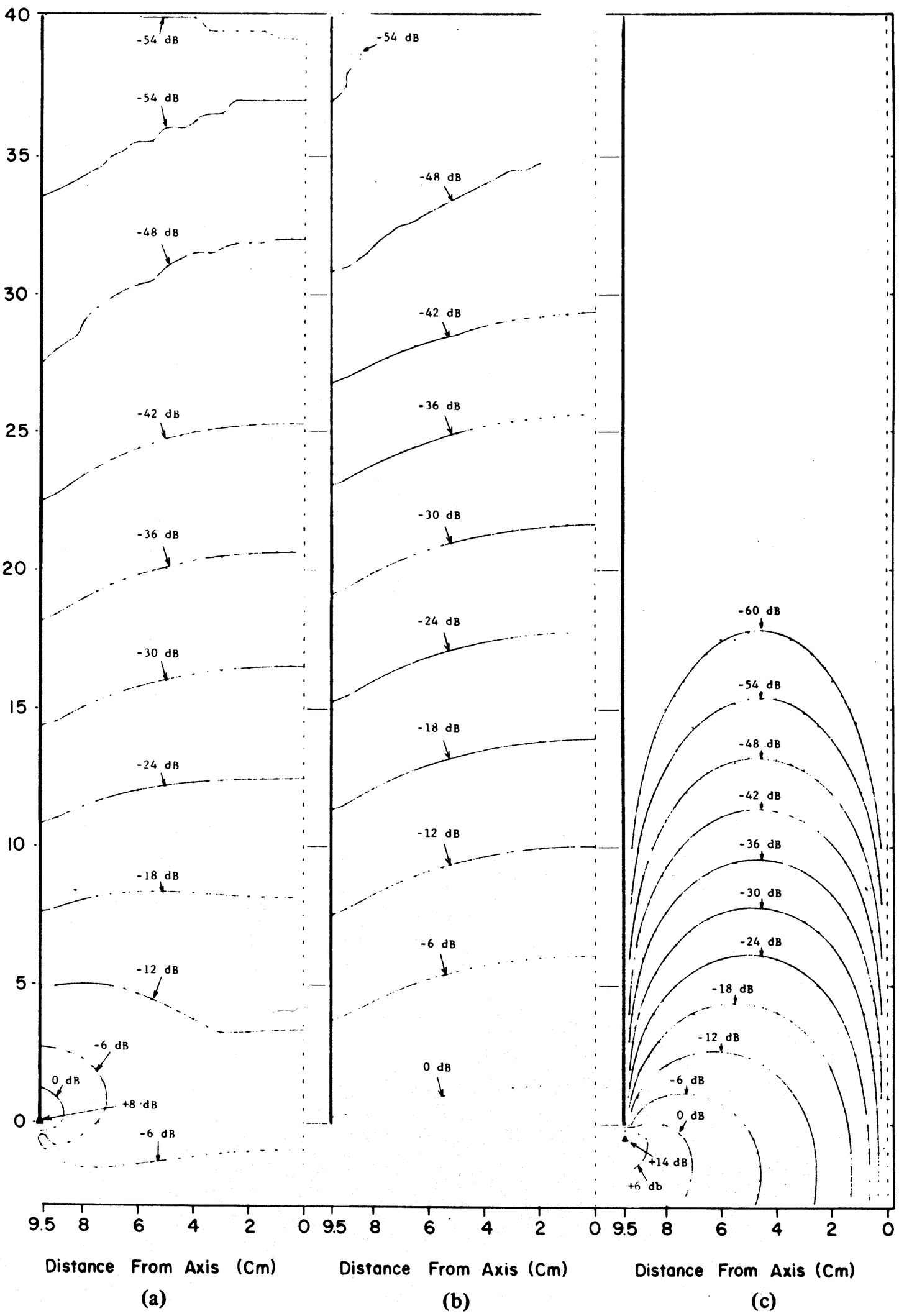

Fig. 8. FD–TD computed field contours in the vertical symmetry plane of the cylinder. (a) E_z. (b) H_x. (c) E_y.

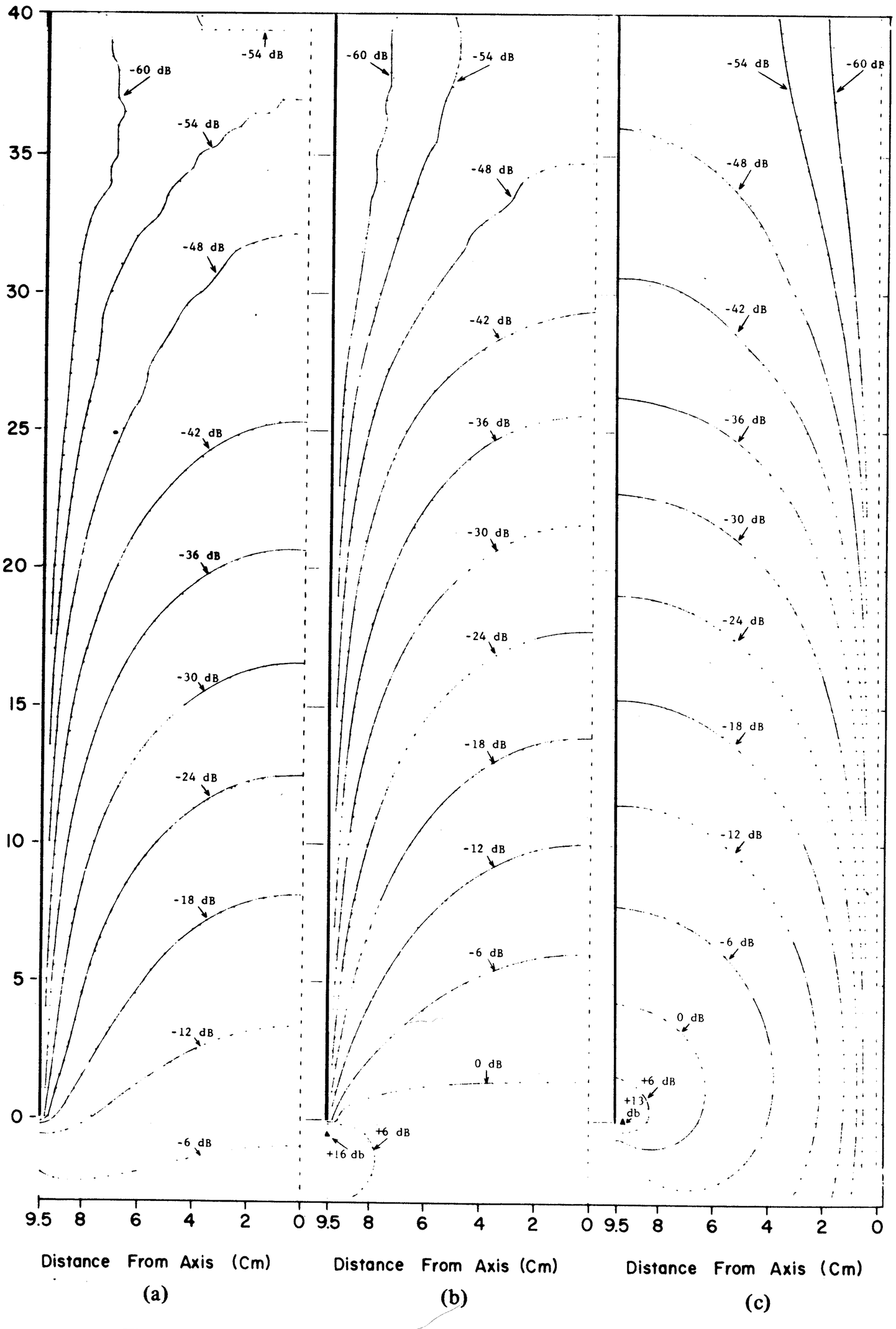

Fig. 9. FD–TD computed field contours in the horizontal symmetry plane of the cylinder. (a) E_z. (b) H_x. (c) H_y.

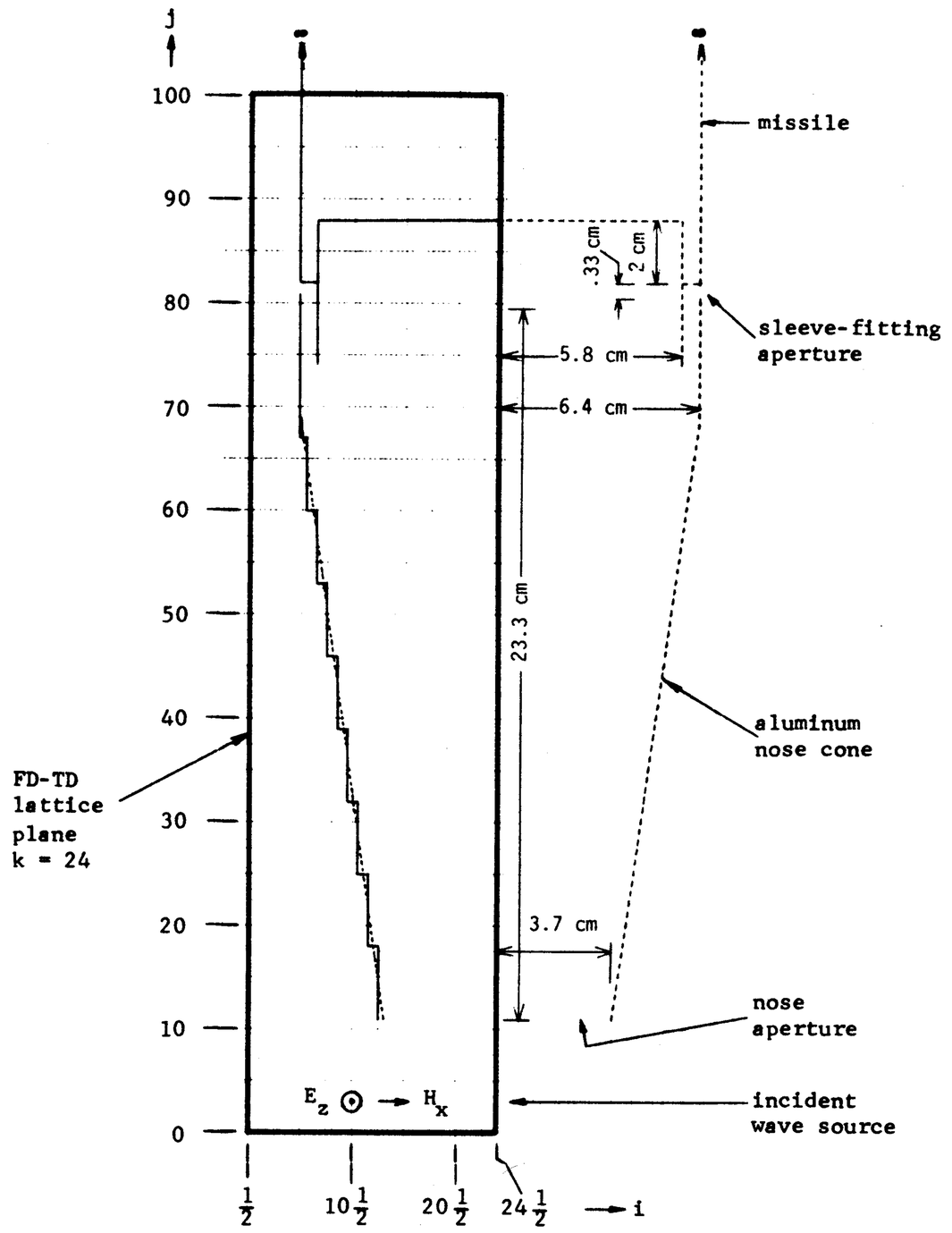

Fig. 10. FD–TD model geometry of an aluminum nose cone with nose aperture and sleeve-fitting aperture, as viewed at lattice plane $k = 24$ (horizontal symmetry plane).

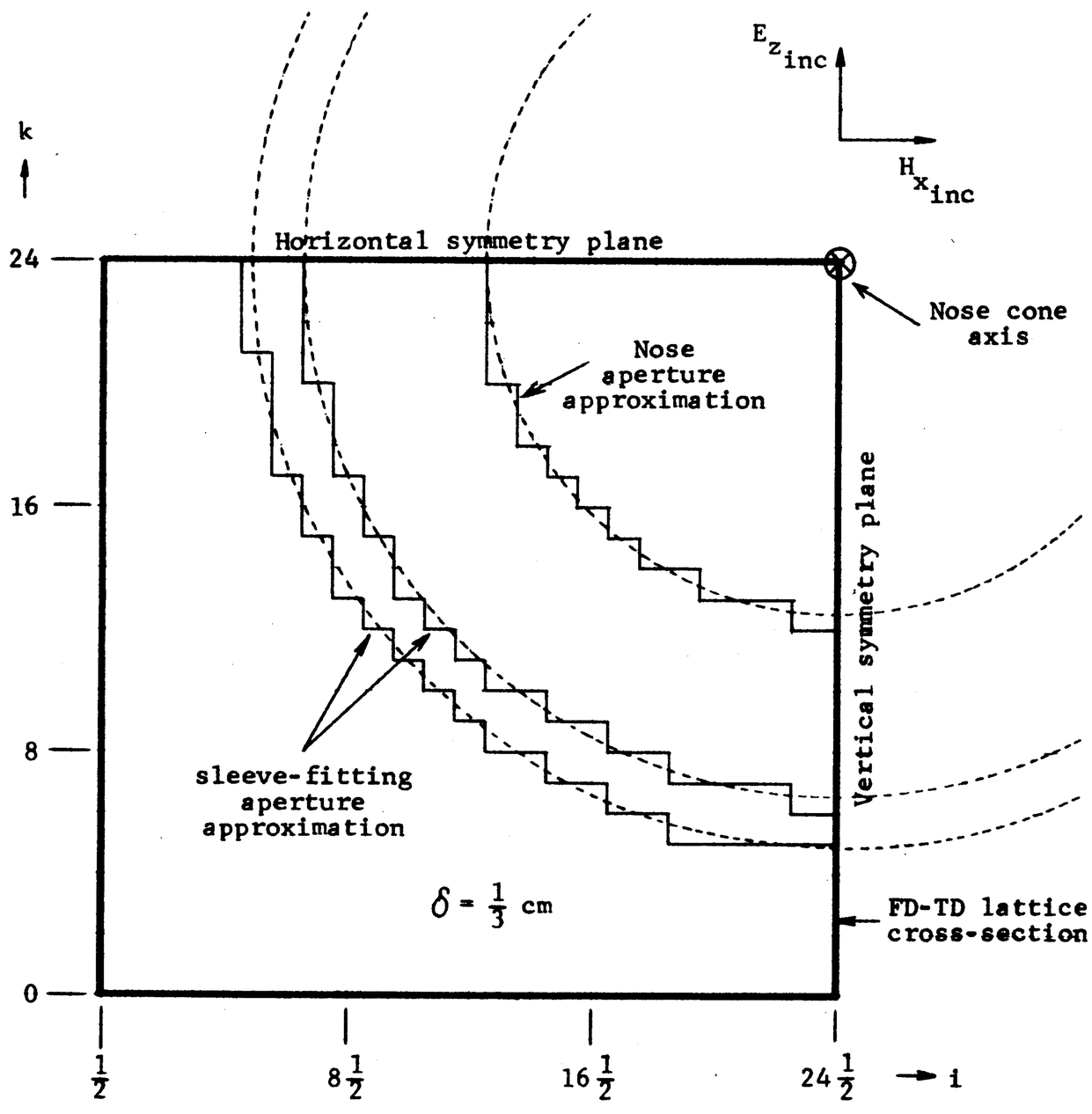

Fig. 11. Transverse cross sections of the nose cone model of Fig. 11.

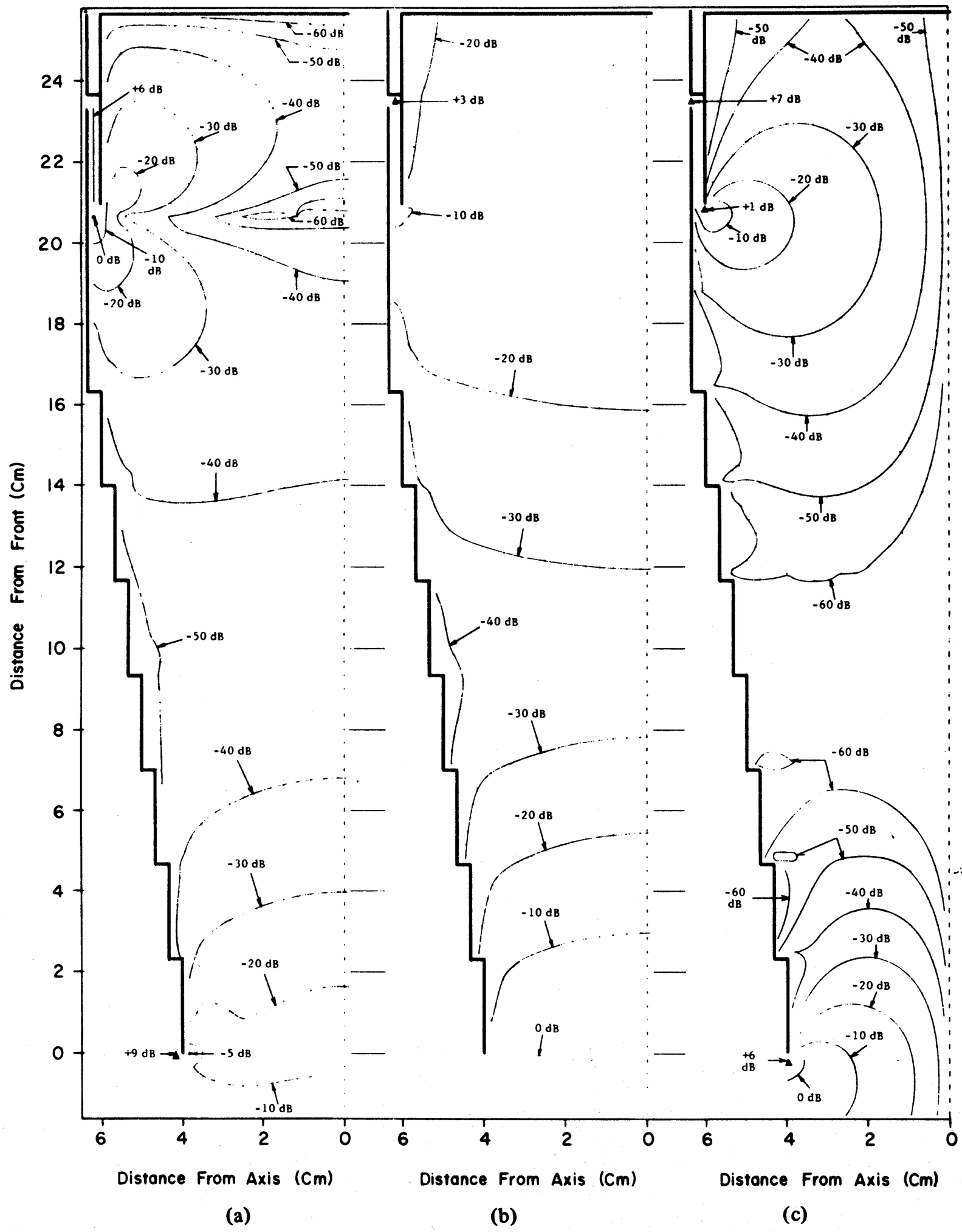

Fig. 12. FD–TD computed field contours in the vertical symmetry plane of the nose cone. (a) E_z. (b) H_x. (c) E_y.

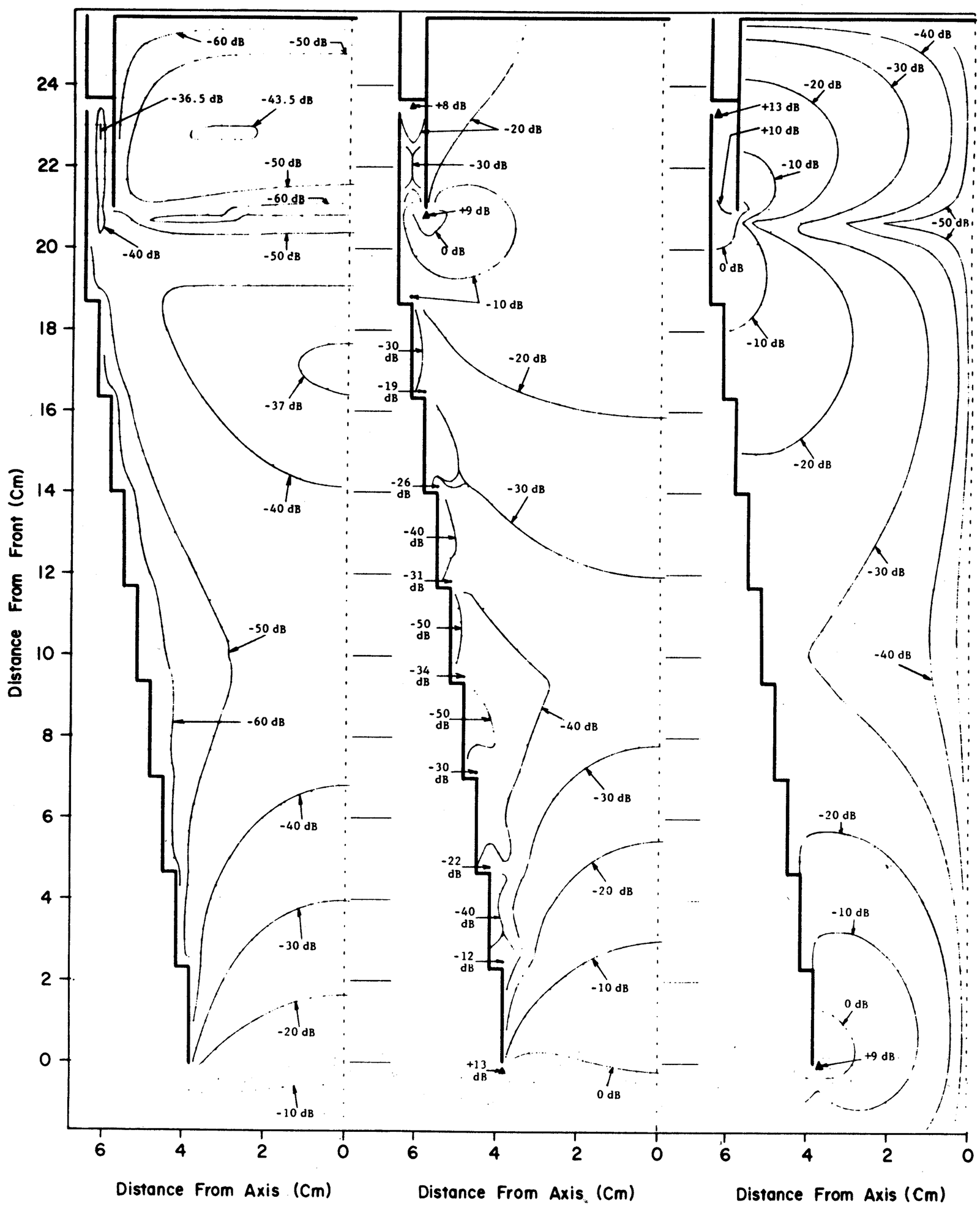

Fig. 13. FD–TD computed field contours in the horizontal symmetry plane of the nose cone. (a) E_z. (b) H_x. (c) H_y.

introduced cusp-like distortions in several of the field contours. However, these distortions were manifested only within about 1 cm of the point of each surface step. Very likely, the exact field contour here can be found simply by drawing a smooth curve connecting the adjacent undisturbed contour sections.

V. DISCUSSION AND CONCLUSIONS

A finite difference-time domain method for predicting the fields within dielectric bodies and metal cavities with apertures has been presented. This approach, called the FD–TD method, has, to this point, demonstrated an accuracy level of ± 1 dB at standing-wave peaks, and ± 1 lattice cell in locating standing-wave peaks and nulls. Within metal structures having beyond-cutoff interiors, convergence of the computed fields to the sinusoidal steady state can occur in less than two periods of the incident wave when a small value of conductivity is assumed for the air of the interior. Program execution times on the order of a few minutes are feasible for problems involving up to 10^6 unknown-field-vector components when using a vector-array-processing computer, such as the Control Data STAR-100.

In future papers reporting the further development of the FD–TD method, applications in the following areas will be discussed:

1) Electromagnetic-wave penetration of metal structures (with apertures) for arbitrary angles of wave incidence and polarization;

2) Wave penetration of combination metal and dielectric structures;

3) Coupling of current to wires and cable bundles within shielded structures;

4) Structuring of a hybrid technique employing both the frequency-domain method of moments and the FD–TD method to predict the fields penetrating complex cavity-backed apertures within large, complex metal structures.

These applications will further delineate the ability of the FD–TD method to achieve realistic models of the sinusoidal steady-state fields penetrating practical structures. Future work will also be directed at generating a user-oriented FD–TD code with three-dimensional geometry-generation features.[1]

REFERENCES

[1] K. S. Yee, "Numerical solution of initial boundary value problems involving Maxwell's equations in isotropic media," *IEEE Trans. Antenna Propagat.*, vol. AP-14, pp. 302–307, May 1966.

[2] E. K. Miller and A. J. Poggio, "Moment-method techniques in electromagnetics from an applications viewpoint," in *Electromagnetic Scattering*, P. L. E. Uslenghi, ed. New York: Academic, 1978, ch. 9.

[3] C. D. Taylor, D.-H. Lam, and T. Shumpert, "Electromagnetic pulse scattering in time-varying inhomogenous media," *IEEE Trans. Antenna Propagat.*, vol. AP-17, pp. 585–589, Sept. 1969.

[4] D. E. Merewether, "Transient currents induced on a metallic body of revolution by an electromagnetic pulse," *IEEE Trans. Electromagn. Compat.*, vol. EMC-13, pp. 41–44, May 1971.

[5] R. Holland, "Threde: A free-field EMP coupling and scattering code," *IEEE Trans. Nucl. Sci.*, vol. NS-24, pp. 2416–2421, Dec. 1977.

[6] A. Taflove and M. E. Brodwin, "Numerical solution of steady-state electromagnetic scattering problems using the time-dependent Maxwell's equations," *IEEE Trans. Microwave Theory Tech.*, vol. MTT-23, pp. 623–630, Aug. 1975.

[7] ——, "Computation of the electromagnetic fields and induced temperatures within a model of the microwave-irradiated human eye," *IEEE Trans. Microwave Theory Tech.*, vol. MTT-23, pp. 888–896, Nov. 1975.

[8] A. Taflove, "Time domain solutions for electromagnetic coupling," Final Rep. RADC-TR-78-142, Contract F30602-77-C-0163, Rome Air Development Center, Griffiss AFB, Rome NY, with IIT Research Inst., Chicago, IL, Illinois, June 1978.

[9] J. A. Stratton, *Electromagnetic Theory*. New York: McGraw-Hill, 1941, pp. 563–573.

[10] D. Wilton and A. Glisson, University of Mississippi, private communication.

[11] H. K. Schuman and D. E. Warren, "Coupling through rotationally symmetric apertures in cavities of revolution," Document RADC-TR-77-214, Rome Air Development Center, Griffiss AFB, Rome, NY, June 1977.

[12] D. E. Warren, Rome Air Development Center, RADC/RBCT, Griffiss, AFB, Rome, NY, private communication.

[1] Present FD-TD codes are available from the author. These codes are, however, research oriented, and may require modification by the user to adapt to his needs.